Gravin regulates centrosome function through PLK1

Erica G. Colicino[a], Alice M. Garrastegui[a,b], Judy Freshour[a], Peu Santra[a], Dawn E. Post[c], Leszek Kotula[c,d], and Heidi Hehnly[a,c,*]

[a]Department of Cell and Developmental Biology, [c]Department of Urology, and [d]Department of Biochemistry, Upstate Medical University, Syracuse, NY 13202, [b]Department of Biology, Syracuse University, Syracuse, NY 13244

ABSTRACT **We propose to understand how the mitotic kinase PLK1 drives chromosome segregation errors, with a specific focus on Gravin, a PLK1 scaffold. In both three-dimensional primary prostate cancer cell cultures that are prone to Gravin depletion and Gravin short hairpin RNA (shRNA)–treated cells, an increase in cells containing micronuclei was noted in comparison with controls. To examine whether the loss of Gravin affected PLK1 distribution and activity, we utilized photokinetics and a PLK1 activity biosensor. Gravin depletion resulted in an increased PLK1 mobile fraction, causing the redistribution of active PLK1, which leads to increased defocusing and phosphorylation of the mitotic centrosome protein CEP215 at serine-613. Gravin depletion further led to defects in microtubule renucleation from mitotic centrosomes, decreased kinetochore-fiber integrity, increased incidence of chromosome misalignment, and subsequent formation of micronuclei following mitosis completion. Murine Gravin rescued chromosome misalignment and micronuclei formation, but a mutant Gravin that cannot bind PLK1 did not. These findings suggest that disruption of a Gravin–PLK1 interface leads to inappropriate PLK1 activity contributing to chromosome segregation errors, formation of micronuclei, and subsequent DNA damage.**

Monitoring Editor
Yukiko Yamashita
University of Michigan

Received: Aug 22, 2017
Revised: Dec 19, 2017
Accepted: Dec 23, 2017

INTRODUCTION

The focus of this study is on understanding the spatial regulation of the mitotic kinase Polo-like kinase 1 (PLK1) during mitosis. This question remains enigmatic due to a multiplicity of PLK1 interactions and substrates located at distinct subcellular sites. Here we examine a PLK1 scaffold protein, Gravin/AKAP12/SSeCKS, that localizes to pericentriolar material (PCM) and cytosol (Gelman, 2010; Hehnly *et al.*, 2015). Gravin has been defined as a scaffold for several kinases (Gelman, 2010). Canton et al. demonstrated in vitro that PLK1 interacts with Gravin through a phosphorylated threonine at 766 (Canton *et al.*, 2012), which validated an earlier proteomics screen that identified Gravin as a possible PLK1 scaffold (Lowery *et al.*, 2007). Gravin depletion was then shown to cause prometaphase delay and chromosome instability through FISH analysis of chromosome 18 (Canton *et al.*, 2012). Gravin also interacts with Aurora A kinase, evidence that Gravin, similarly to CEP192 (Joukov *et al.*, 2014) and Bora (Chan *et al.*, 2008), has the potential to facilitate a mitotic signaling cascade between Aurora A and PLK1 (Hehnly *et al.*, 2015). The direct interactions and localization patterns of Gravin and PLK1 were previously characterized (Canton *et al.*, 2012; Hehnly *et al.*, 2015). However, these studies did not thoroughly examine or definitively determine how, in live cells, Gravin regulates PLK1 distribution, activity, or downstream function, which is the main focus of this study.

PLK1 misregulation can drive chromosome missegregation and subsequent formation of micronuclei (Lera and Burkard, 2012). Micronuclei are structures formed as a result of lagging chromosomes that contain either whole or partial chromosomes outside of the

This article was published online ahead of print in MBoC in Press (http://www.molbiolcell.org/cgi/doi/10.1091/mbc.E17-08-0524) on December 27, 2017.

The authors declare that they have no conflict of interest.

Author contributions: E.C., P.S., and A.G. designed and conducted experiments and analyzed the data under the supervision of H.H.; J.F. constructed all viral vectors; D.P. maintained primary prostate cancer cell lines and is under the supervision of L.K.; technical expertise was provided by L.K. and D.P.; E.C. and H.H. wrote the manuscript; all authors critically read and contributed to the manuscript.

*Address correspondence to: Heidi Hehnly (hehnlyh@upstate.edu).

Abbreviations used: DAPI, 4,6-diamidino-2-phenylindole; EGF, epidermal growth factor; EGTA, ethylene glycol-bis(β-aminoethylether)-*N*,*N*,*N*′,*N*′-tetraacetic acid; FRAP, fluorescence recovery after photobleaching; FRET, fluorescence resonance energy transfer; HEK, human embryonic fibroblasts; LB, lysis buffer; MEF, mouse embryonic fibroblasts; PACT, pericentrin-AKAP450-centrosomal targeting domain; PCM, pericentriolar material; PLK1, Polo-like kinase 1; RPE, retinal pigmented epithelium; shRNA, short hairpin RNA; SIM, structured illumination microscopy; STED, stimulated emission depletion microscopy.

macronucleus (Crasta *et al.*, 2012). Abnormal mitotic kinase expression and activity, such as with PLK1, has been linked to genomic instability in prostate cancer (Deeraksa *et al.*, 2013). Microarray-based studies demonstrated a 3- to 10-fold reduction in relative Gravin mRNA levels in breast, prostate, lung, ovarian, testicular, and other cancer types compared with controls (Gelman, 2010). One plausible mechanism to generate substantial local mutagenesis observed in prostate cancer is physical isolation of one or two chromosomes and their partition into micronuclei. Chromosomes in micronuclei can be subject to massive DNA damage (Holland and Cleveland, 2012). Here we are testing the hypothesis that Gravin loss inappropriately distributes PLK1 signaling during mitosis, driving chromosome missegregation that leads to formation of micronuclei.

RESULTS AND DISCUSSION

Gravin loss is associated with increased formation of micronuclei in primary prostate cancer cells

We first analyzed primary hormone therapy–resistant prostate epithelial cells in three-dimensional (3-D) cultures (derived from Gao *et al.*, 2014) in parallel with an immortalized prostate epithelial cell line, RWPE-1. Using this system, we found that Gravin can be significantly down-regulated in primary prostate cancer cells. By comparing two primary patient samples, PCa1 and PCa3, with an immortalized prostate epithelial cell line, RWPE-1, or a control primary prostate epithelial cell line, 26Na, we found that Gravin expression is diminished in PCa1 (Figure 1A). When 3-D primary cultures (Figure 1, A–E) and prostate epithelial cells genetically modified using Gravin short hairpin RNA (shRNA) (Figure 1, F–H) were compared, an increase in mitotic delay or formation of micronuclei was noted in cells that lacked Gravin. Specifically, PCa1 cells that display a significant reduction in Gravin expression (Figure 1A) had an increase in mitotic index compared with both control and PCa3 cells (Figure 1, B and D). PCa1 also contained 25.04 ± 2.35% of cells containing micronuclei compared with 2.65 ± 1.10% in controls and 10.43 ± 3.93% in PCa3 (Figure 1, C and E). These results suggest that Gravin loss contributes to formation of micronuclei in PCa1. From this, we wanted to know whether the effects of Gravin loss on micronuclei formation are the result of inappropriate PLK1 distribution and/or activity causing chromosome missegregation.

Gravin loss disrupts PLK1 dynamics predominately at mitotic centrosomes

It is unclear how the loss of Gravin impacts PLK1 in live cells during mitosis. One possibility is that scaffold proteins, such as Gravin, help coordinate the appropriate spatial organization of PLK1 to direct the flow of molecular information. Previous studies identified that Gravin phosphorylation at T766 primes it for PLK1 binding (modeled in Figure 2A) and this interaction takes place, at least in part, at mitotic centrosomes (Canton *et al.*, 2012; Hehnly *et al.*, 2015). However, these studies did not examine how this interaction regulates the spatial and temporal dynamics of PLK1 in live cells. By structured illumination microscopy (SIM), we confirmed the finding of our previous studies (Hehnly *et al.*, 2015) that Gravin localizes to mitotic centrosomes (Figure 2B, a′, orange arrows*) along with PLK1 (Figure 2B, b′, orange arrows). Additionally, PLK1 localizes to kinetochores (Figure 2B, b′, magenta arrow) and later in mitosis at the cytokinetic midbody (Figure 2C). Owing to the similar localization patterns of Gravin and PLK1 at mitotic centrosomes, we predict that Gravin loss may disrupt PLK1 dynamics at this locale in live cells during mitosis.

We first examined whether there was a difference in PLK1 dynamics between the mitotic centrosomes, kinetochores, and cytokinetic midbody. A previous study carefully compared the fluorescence recovery after photobleaching (FRAP) kinetics of PLK1 at each of these locales by overexpression of GFP-PLK1 and analysis at 30°C in a human osteosarcoma cell line, U2OS (Kishi *et al.*, 2009). Instead of transiently expressing PLK1, we utilized a cell line with normal ploidy expressing a PLK1 shRNA to eliminate endogenous PLK1 and exogenously expressed an shRNA resistant GFP-PLK1 at endogenous levels (RPE cells, Figure 2C). In addition, FRAP analysis was performed at 37°C. Similarly to the previous study (Kishi *et al.*, 2009), we found significantly different dynamics between mitotic centrosomes, kinetochores, and the cytokinetic midbody for GFP-PLK1 (Figure 2, C and D; Supplemental Figure S1A). However, the half-life of PLK1 at each of these locales was considerably shorter than reported in Kishi *et al.* (2009) (Figure 2D). We predict that this is the case due to endogenous expression levels of PLK1 and 37°C incubation.

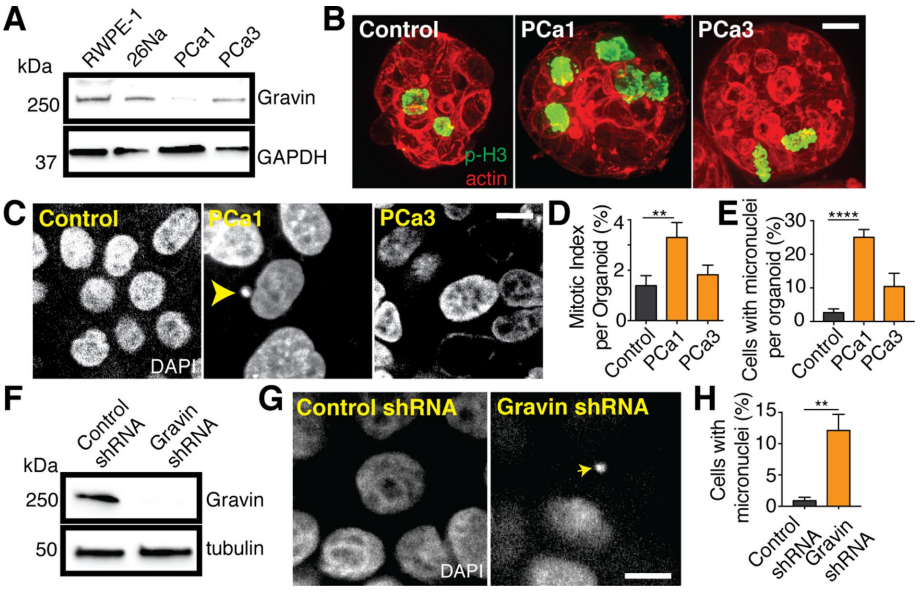

FIGURE 1: Gravin loss is associated with increased micronuclei formation in primary prostate cancer cells. (A) Immunoblot analysis showing decreased Gravin expression in PCa1 and PCa3 cancer cells in comparison with RWPE-1 and normal patient prostate epithelium cells (26Na). (B) Control (RWPE-1), PCa1, and PCa3 3-D acini cultures fluorescently labeled for p-H3 (green) and actin (red). (C) Control (RWPE-1), PCa1, and PCa3 3-D acini labeled for DAPI (gray) displaying micronuclei within a single cell (yellow arrowhead). Confocal micrographs for B and C are presented as maximum projections. Bar, 5 μm. (D, E) Quantification of the mitotic index (D) and cells (%) with micronuclei (E) for control (RWPE), PCa1, and PCa3 in 3-D acini was calculated. $n = 30$ organoids over $n = 3$ experiments ± SEM, Student's t test $p = 0.0099$ (D) and $p < 0.0001$ (E). (F) Immunoblot analysis of Gravin expression in RWPE-1 cells expressing a control GAPDH shRNA or a Gravin shRNA. Tubulin was used as loading control. (G) Control shRNA and Gravin shRNA RWPE-1 3-D acini cultures stained for DAPI displaying micronuclei within a single cell (yellow arrow). Bar, 5 μm. (H) Quantification of Gravin shRNA and control shRNA treated cells with micronuclei (%) over $n = 3$ experiments ± SEM. Student's t test $p = 0.0097$.

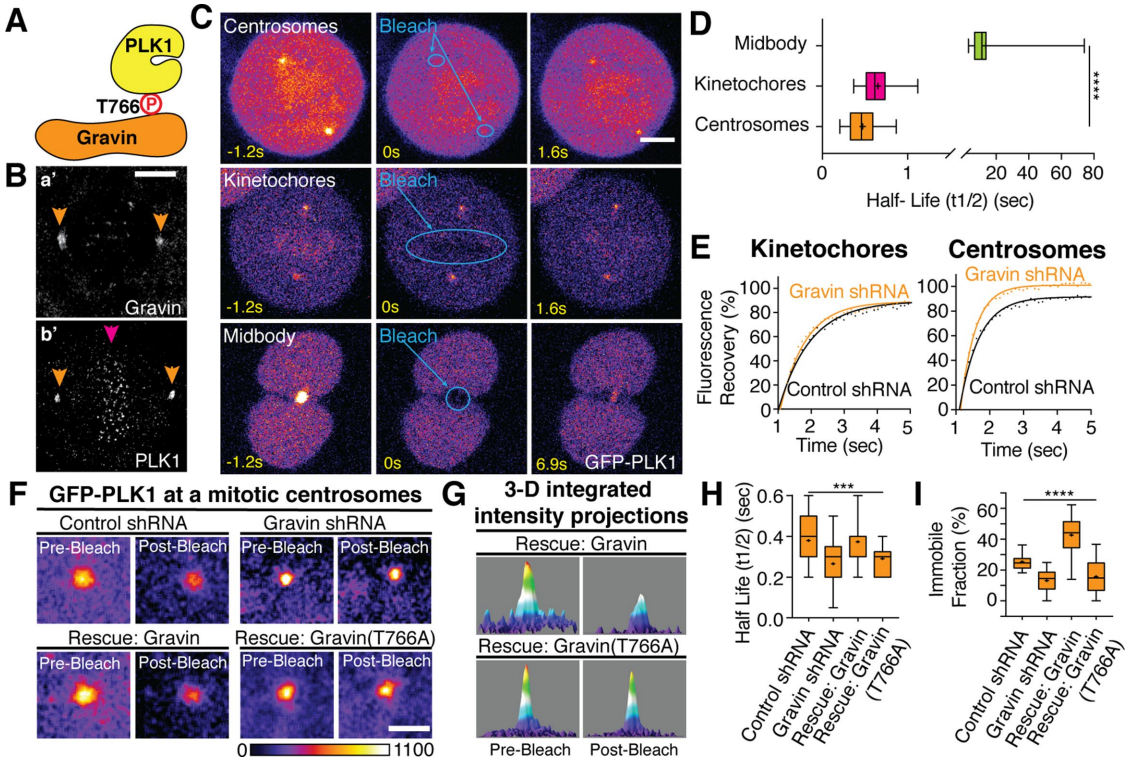

FIGURE 2: Gravin loss disrupts PLK1 dynamics predominately at mitotic centrosomes. (A) Model depicting Gravin (orange) binding PLK1 (yellow) at phosphorylated T766 (Canton *et al.*, 2012). (B) Maximum projection of structured illumination microscopy (SIM) micrographs of Gravin (a') and PLK1 (b') localizing to mitotic centrosomes (orange arrows) in metaphase cells. Magenta arrow represents PLK1 localization at kinetochores in b'. (C) Representative images of fluorescence recovery after photobleaching (FRAP) of GFP-PLK1 (Fire LUT, ImageJ) RPE cells at mitotic centrosomes, kinetochores, and cytokinetic midbodies. Bar, 5 μm. (D) Quantification presented as box-and-whisker plot of half-life for GFP-PLK1 in control and Gravin-shRNA treated cells (+ indicates mean, $n > 20$ cells across $n = 3$ experiments, ANOVA indicates significance of $p < 0.0001$). (E) A curve was fitted using one-phase decay of PLK1 fluorescence recovery at kinetochores (left) and mitotic centrosomes (right) in metaphase cells treated with control or Gravin shRNAs ($n > 20$ cells over $n = 3$ experiments). (F) GFP-PLK1 at a single metaphase mitotic centrosome in control shRNA- or Gravin shRNA-treated cells rescued with full-length wild-type Gravin, or T766A mutant Gravin prior to and 3 s after bleaching events. Confocal micrographs at a single mitotic centrosome are shown (Fire LUT, Image J, bar indicates gradient of integrated fluorescence intensity values, A.U.). Bar, 2 μm. (G) Integrated intensity profiles for GFP-PLK1 at a single mitotic centrosome before and 3 s after bleaching events are presented. (H, I) The average (H) half-life ($t_{1/2}$) and (I) immobile fraction of GFP-PLK1 at metaphase spindle poles was calculated and presented as box-and-whisker plots with + indicating mean ($n > 20$ cells over $n = 3$ experiments). One-way ANOVA indicates significance between $p < 0.001$ (H) and $p < 0.0001$ (I).

We next compared GFP-PLK1 dynamics in Gravin-depleted RPE cells (Gravin shRNA) and in control RPE cells (control shRNA; Supplemental Figure S1B). Gravin-depleted cells had a significant decrease in GFP-PLK1 half-life at kinetochores (Figure 2E; Supplemental Figure S1, C and D) and mitotic centrosomes (Figure 2, E and H) and no significant difference at cytokinetic midbodies (Supplemental Figure S1, F and G). We then compared the immobile fraction of GFP-PLK1 at each locale, that is, the fraction of GFP-PLK1 that remained after photobleaching. Gravin-depleted cells demonstrated a 12% decrease in the immobile fraction at mitotic centrosomes when compared with controls (Figure 2, E and I). However, no difference in the immobile fraction was observed at kinetochores or at the cytokinetic midbody (Figure 2E; Supplemental Figure 1, E and H).

Using control and Gravin-depleted cells rescued ectopically with wild-type Gravin or Gravin (T766A) that cannot bind PLK1 (Canton *et al.*, 2012), we repeated the FRAP experiments at individual mitotic centrosomes (Figure 2, F and G; expression levels following rescues in Supplemental Figure S1B). A significant proportion of GFP-PLK1 fluorescence was not recovered at mitotic centrosomes in control shRNA and Gravin-rescued cells, representing the immobile fraction of PLK1. In Gravin-depleted and Gravin (T766A) rescue cells, GFP-PLK1 fluorescence is almost fully recovered 3 s post-bleach (Figure 2, F and G). From analysis of multiple metaphase cells, rescue with Gravin (T766A) caused a significant decrease in the immobile fraction and in the half-life of GFP-PLK1 compared with wild-type Gravin rescue (Figure 2, H and I). With wild-type Gravin rescue there is a slight increase in total Gravin expression compared with that in controls, which is likely causing the significant increase in the immobile fraction of GFP-PLK1 (42.68% immobile) compared with that for control shRNA (25.33% immobile, Figure 2I). Collectively, these findings suggest that GFP-PLK1 dynamics at mitotic centrosomes is partly regulated by its binding scaffold Gravin.

Gravin-depleted cells redistribute active PLK1, causing increased phosphorylation events at mitotic centrosomes

We utilized a fluorescence resonance energy transfer (FRET)-based phosphorylation sensor (Macůrek *et al.*, 2008) to test whether Gravin loss causes a change in PLK1 activity. The PLK1 biosensor is

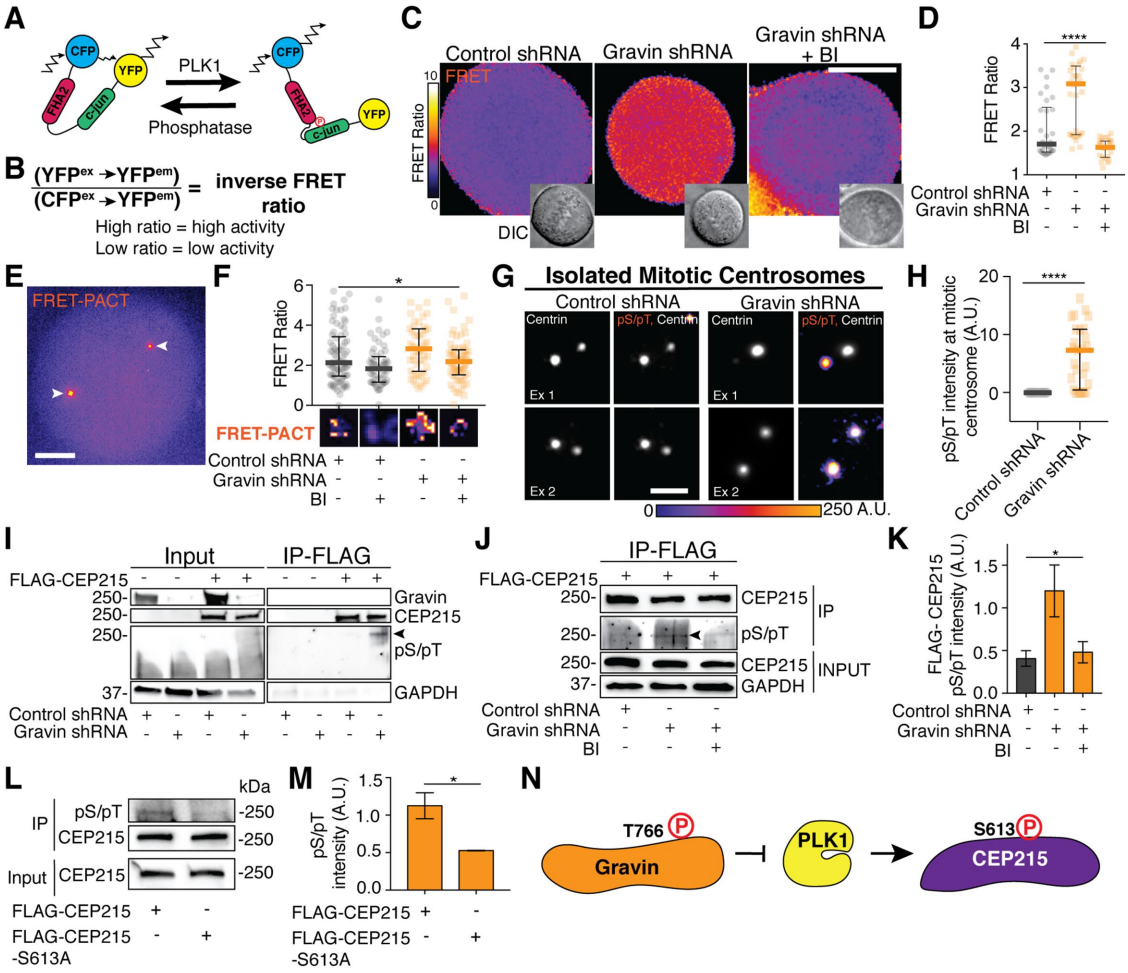

FIGURE 3: Gravin-depleted cells redistribute active PLK1, causing increased phosphorylation events at mitotic centrosomes. (A) Model of PLK1 biosensor showing how increased PLK1 activity causes a conformational change in the biosensor through phosphorylation of c-jun (green) and binding of the FHA2 domain (magenta), resulting in a loss of FRET. When there is increased phosphatase activity, the PLK1 biosensor is in a relaxed state, allowing FRET. (B) Equation for determining the inverse FRET ratio by dividing the $YFP^{EX} \rightarrow YFP^{EM}$ by the $CFP^{EX} \rightarrow YFP^{EM}$. When the inverse FRET ratio is calculated, high ratios correspond with high levels of PLK1 activity while low ratios correspond to low levels of PLK1 activity. (C) Relative PLK1 activity shown as an inverse FRET ratio (Fire LUT, ImageJ, bar indicates gradient of FRET ratio values) and DIC images taken from nocodazole synchronized and released cells in metaphase. Control shRNA, Gravin shRNA, and Gravin shRNA cells plus BI2536 are shown. Bar, 5 µm. (D) Quantification of the inverse FRET efficiency nocodazole-released cells in metaphase that were treated with control shRNA, Gravin shRNAs, and/or BI2536 (BI) is presented as a scatterplot. $n > 30$ cells over $n = 3$ experiments, median with interquartile range shown, one-way ANOVA $p < 0.0001$. (E) PLK1-FRET-PACT biosensor localization in metaphase cells. Arrows depict mitotic centrosomes (Fire LUT). Bar, 5 µm. (F) The inverse FRET-efficiency of the PLK1-FRET-PACT probe was quantified from nocodazole synchronized and released metaphase cells treated with control shRNA, Gravin shRNA, and/or BI2536 (BI) and presented as a scatterplot. Representative single mitotic centrosome inverse FRET ratios shown below graph (FIRE-LUT). $n > 50$ cells over $n = 4$ experiments, median with interquartile range shown, one-way ANOVA $p = 0.0371$. (G) Isolated mitotic centrosomes from control shRNA and Gravin shRNA HEK293 cells immunolabeled for centrin (white) and phosphoserine/phosphothreonine (pS/pT; FIRE LUT). Bar, 2 µm. (H) Quantification of pS/pT intentsity at mitotic centrosomes in G presented as a scatterplot. $n = 27$ centrioles for each treatment, median with interquartile range shown, Student's t test $p < 0.0001$. (I, J) FLAG IP of Mock or FLAG-CEP215 transfected control shRNA- or Gravin shRNA ± BI2536-treated HEK293 cells as indicated. Protein expression and immunoprecipitation was analyzed by immunoblot for Gravin, CEP215, pS/pT, and GAPDH (as loading control). Black arrowhead indicates pS/pT band at 250 kDa. (K) Quantification of pS/pT intensities normalized over total FLAG-CEP215 IP ($n = 3$ experiments ± SEM, one-way ANOVA $p = 0.0353$). (L) Immunoblot analysis of FLAG-CEP215 and FLAG-CEP215-S613A IP from HEK293 cells. (M) Quantification of pS/pT expression levels from FLAG-IP normalized over total FLAG-CEP215 ($n = 3$ experiments ± SEM, Student's t test $p = 0.0264$). (N) Working model depicting that phosphorylated Gravin (orange) inhibits PLK1 (yellow) from phosphorylating CEP215 (purple) during mitosis.

composed of a monomeric CFP and YFP flanking a PLK1 specific c-jun substrate sequence tethered by a flexible linker to an FHA2 phosphothreonine binding domain (Liu *et al.*, 2012). The phosphorylation of the PLK1 substrate triggers an intramolecular clamp with the FHA2, causing a conformational change that decreases the amount of FRET from CFP to YFP (Figure 3A). The FRET biosensor

provides a fluorometric readout for PLK1 phosphorylation, and a decrease in FRET is measured upon increased activity of PLK1. For ease of interpretation, we plotted an inverse ratio of $YFP^{EX}\rightarrow YFP^{EM}$ over $CFP^{EX}\rightarrow YFP^{EM}$ (Figure 3B), so that an increase in the inverse FRET ratio represents an increase in PLK1 activity. To determine whether anchoring of PLK1 by Gravin affected PLK1's activity, we monitored either the PLK1 biosensor in cycling cells (Supplemental Figure S2, A and B) or cells synchronously released from mitotic arrest by nocodazole (Figure 3, C and D; Supplemental Figure S2C). For these studies we utilized HEK293 cells treated with either a control shRNA or Gravin shRNA with or without addition of the PLK1 inhibitor BI2536. In control cells treated with BI2536 a significant decrease in the inverse FRET ratio was calculated (Supplemental Figure S2C), suggesting that we accurately measured PLK1 activity. In cells depleted of Gravin, a significant increase in the inverse FRET ratio was calculated when compared with that in control cells (median of 1.703 compared with 3.09 for Gravin-depleted cells, Figure 3, C and D), and the increase was lost after treatment with the PLK1 inhibitor BI2536, indicating that the increase requires PLK1 kinase activity (median of 1.63, Figure 3, C and D). Previous studies reported that an upstream PLK1 kinase, Aurora A, activates PLK1 during mitosis by phosphorylating it at T210 (Macůrek *et al.*, 2008). This is facilitated by these two kinases forming a complex with Gravin. We confirmed that Gravin loss resulted in a modest decrease in T210 phosphorylation (Hehnly *et al.*, 2015; Supplemental Figure S2, D and E). However, Gravin loss caused a significant increase in the FRET-biosensor fluorometric readout (Figure 3, C and D). One possibility is that Gravin-depleted cells display a slight decrease in global PLK1 activity, shown by decreased phosphorylation at T210; however, a population of active PLK1 is redistributed in cells, allowing increased phosphorylation and unregulated access to its substrates. Thus, we conclude that we are not causing an increase in overall activity of PLK1, but a change in distribution of already active PLK1 with Gravin loss.

Since Gravin and PLK1 likely interact on mitotic centrosomes (Figure 2, B and E; Hehnly *et al.*, 2015), we tested for changes in PLK1 centrosome substrate phosphorylation with loss of Gravin. To mimic the localization of possible endogenous PLK1 centrosome substrates, we attached a pericentrin-AKAP450-centrosomal-targeting domain (PACT) to the c-terminus of the FRET biosensor (FRET-PACT), which successfully targets the PLK1 biosensor to mitotic centrosomes (Figure 3E). To examine FRET-PACT response to changes in PLK1 activity in living cells, we imaged mitotic HEK293 cells treated with a control shRNA, Gravin shRNA, and/or the PLK1 inhibitor, BI2536. As with the cytosolic PLK1 FRET biosensor, the centrosome-targeted biosensor demonstrated a significant increase in the inverse FRET ratio in Gravin-depleted cells (median of 2.83) compared with controls (median of 2.13; Figure 3F). Treatment with BI2536 decreased the FRET ratio for both control cells (median of 1.84) and Gravin-depleted cells (median of 2.18; Figure 3F).

We confirmed the increase in phosphorylation seen with the FRET-PACT biosensor by isolating mitotic centrosomes (Hung *et al.*, 2015) from control and Gravin-depleted cells. Gravin-depleted mitotic centrosomes displayed a significant increase in phosphoserine/phosphothreonine (pS/pT) compared with controls (Figure 3, G and H). We next examined a putative centrosome-localized PLK1 substrate, CEP215 (Santamaria *et al.*, 2011), for increased phosphorylation in Gravin-depleted cells compared with controls (Figure 3I). Immunoblot analysis detected a threefold increase in PLK1-dependent pS/pT levels in FLAG-CEP215 isolated from Gravin shRNA–treated cell lysate compared with control lysate or lysates treated with BI2536 (Figure 3, I–K). A previous phosphoproteomics screen of PLK1 substrates identified a PLK1 phosphorylation site on CEP215 at its serine-613 residue (Santamaria *et al.*, 2011). Through sequence alignment, we found that this serine is conserved between human and murine CEP215 (Supplemental Figure S2F). We immunoprecipitated a FLAG-tagged nonphosphorylatable mutant, CEP215 (S613A), or wild-type FLAG-CEP215, and FLAG-CEP215-S613A presented with decreased pS/pT phosphorylation compared with FLAG-CEP215 (Figure 3, L and M), suggesting that serine-613 is phosphorylated. Collectively, these data support the idea that Gravin constrains a subset of PLK1 to be released at the right time and place. When Gravin is depleted, this subset of PLK1 is now free to inappropriately phosphorylate downstream substrates, one of which is CEP215 at serine 613 (modeled in Figure 3N).

Gravin loss results in CEP215 disorganization and disrupted mitotic centrosome function

Since CEP215 phosphorylation is increased in Gravin-depleted cells, we examined if its organization at the mitotic centrosomes was affected in HEK293 cells treated with Gravin shRNA. Using stimulated emission depletion microscopy (STED), CEP215 in control cells clustered into a ring-like structure at both mitotic centrosomes (Figure 4A). In Gravin-depleted cells, we found that CEP215 no longer organized symmetrically across the two poles. One pole contained more CEP215 that was no longer organized in a ring and the other pole contained diffusely arranged CEP215. Line scans across multiple cells that bisected the mitotic centrosomes demonstrated a specific decrease in CEP215 organization on one pole over the other in Gravin-depleted cells compared with controls (Figure 4A). We then measured the fluorescence intensity of CEP215 at mitotic centrosomes in cells treated with either control or Gravin shRNA. Gravin-depleted cells contained significantly less CEP215 at mitotic centrosomes than controls (Figure 4B). When the ratio of the mitotic centrosome with the highest CEP215 fluorescence intensity to the mitotic centrosome with the lowest was calculated, Gravin-depleted cells had a significantly higher ratio (Figure 4C). Together, these data suggest that Gravin loss causes decreased CEP215 organization and localization at mitotic centrosomes, leading to an asymmetric distribution of CEP215 between the two mitotic centrosomes.

To determine whether Gravin loss and subsequent CEP215 disorganization and distribution lead to defects in centrosome function, we performed a functional test to monitor mitotic centrosome–mediated MT-nucleating activity over time in HEK293 cells. Spindles were disassembled with nocodazole and examined at different times after nocodazole washout for MT nucleation. At 0 min there was less tubulin at mitotic centrosomes in Gravin-depleted cells than in controls. At 2 min of regrowth, mitotic centrosomes in control cells showed an increased ability to nucleate MTs (Figure 4, D and E). This activity was modestly impaired at first in Gravin-depleted cells, but by 5 min both Gravin-depleted cells and control cells were nucleating MTs to a similar degree, and by 20 min Gravin-depleted cells formed a complete spindle, whereas control cells were still recovering from the regrowth (Figure 4D). This finding suggests that the initial defects in nucleation at 0 and 2 min could be caused by downstream defects in PLK1 target organization, such as CEP215, which is known to organize the γ-tubulin ring complex (Fong *et al.*, 2008). Following this, the redistribution of active PLK1 caused by Gravin loss likely contributes to the rapid increase in nucleation and spindle assembly after nocodazole washout (Figure 4, D and E). One possible consequence for defects in centrosome function and/or abnormal PLK1 activity is a loss in kinetochore fiber integrity (Paschal *et al.*, 2012; Hehnly and Doxsey, 2014). To test whether Gravin loss affects kinetochore fiber integrity, we employed

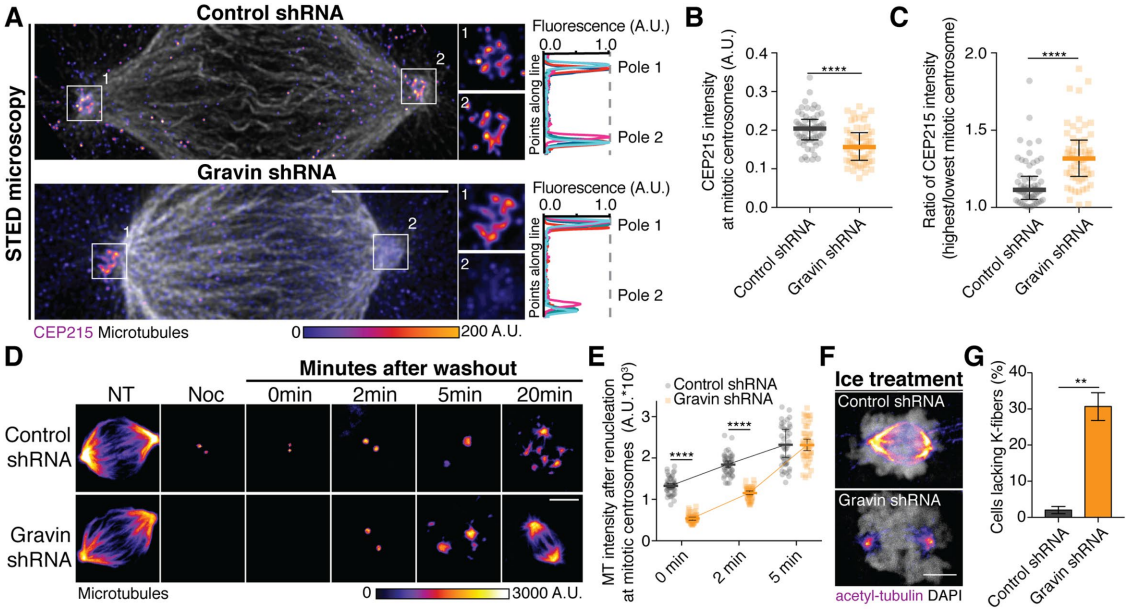

FIGURE 4: Gravin loss results in CEP215 disorganization and disrupted mitotic centrosome function. (A) STED (stimulated emission–depletion) micrographs of metaphase control and Gravin shRNA HEK293 cells are presented as maximum projections. Cells were immunostained for CEP215 (Fire-LUT, ImageJ, bar indicates gradient of integrated fluorescence intensity values, A.U.) and tubulin (white). Bar, 5 μm. Inserts (white boxes) depict 2× magnification of CEP215 at mitotic centrosomes. A line scan through the mitotic centrosomes is drawn and the normalized fluorescence intensity of CEP215 is plotted (right, each line represents a single line scan over $n = 5$ cells for each treatment). (B) Quantification of total CEP215 fluorescence intensity at mitotic centrosomes in control and Gravin shRNA–treated HEK293ad cells. $n = 3$ experiments, $n = 60$ cells, median with interquartile range shown, Student's t test, $p < 0.0001$. (C) Ratio of highest CEP215 intensity over lowest CEP215 intensity between the two mitotic centrosomes within a single cell. $n = 60$ cells over $n = 3$ experiments, median with interquartile range shown, Student's t test $p < 0.0001$. (D) A series of confocal micrographs demonstrating MT regrowth (α-tubulin, Fire-LUT, bar indicates gradient of integrated fluorescence intensity values, A.U.) at mitotic centrosomes for a time course following nocodazole washout in HEK293 cells treated with Gravin or control shRNAs. Micrographs presented as maximum projections. Bar, 5 μm. (E) The integrated α-tubulin intensity at mitotic centrosomes was quantified and presented as a scatterplot at indicated times following washout. $n = 50$ poles for each time and treatment, median with interquartile range shown, representative of $n = 3$ experiments, Student's t test for 0 min ($p < 0.0001$), 2 min ($p < 0.0001$), and 5 min ($p = 0.60$). (F) Maximum confocal projections of control shRNA and Gravin shRNA mitotic HEK293 cells treated for 5 min on ice. Cells were immunostained for acetylated tubulin (Fire-LUT, ImageJ) and DAPI (white). (G) Quantification of cells (%) lacking K-fibers in HEK293 cells treated with control or Gravin shRNAs calculated over $n = 3$ experiments ± SEM (Student's t test $p = 0.0020$).

cold treatment to specifically eliminate dynamic microtubules from mitotic HEK293 cells. Kinetochore fibers in control cells were well organized and robust (Figure 4F). Following Gravin depletion, kinetochore fibers were completely lost in 31 ± 3.84% of mitotic cells (Figure 4G). A previous study reported that an active form of PLK1, PLK1 T210D, resulted in labile kinetochore fibers, in contrast to wild-type controls (Paschal *et al.*, 2012). This finding, in combination with our findings, suggests that redistribution of active PLK1 caused by Gravin loss disrupts centrosome function and kinetochore fiber integrity.

Gravin loss and increased phosphorylation of CEP215 results in higher incidence of cells containing micronuclei

PLK1 is an essential kinase in the regulation of mitotic progression by allowing the passage of cells through the G2/M cell cycle checkpoints (Zitouni *et al.*, 2014). Premature passage of these checkpoints through overactive PLK1 has been shown to cause genomic instability in cells through lagging chromosomes and DNA damage (Pan *et al.*, 2009). In addition, a disruption in centrosome function through the loss of centrioles also results in increased lagging chromosomes and micronuclei formation (Sir *et al.*, 2013). Thus, we examined whether Gravin-depleted cells, which have decreased centrosome function (Figure 4, D and E), present with lagging chromosomes. Comparing 3-D prostate epithelial cells depleted of Gravin with controls, we noted an increase in lagging chromosomes (Supplemental Figure S3A). To monitor this quantitatively in live cells, we utilized a GFP-H2B HeLa cell line stably depleted of Gravin (Gravin shRNA; Supplemental Figure S3, B–D), where only 42.28 ± 11.20% of Gravin-depleted cells displayed normal chromosome alignment, compared with 81.16 ± 6.90% of control cells. Of the remaining cells, 32.37 ± 6.17% of dividing Gravin-depleted cells presented with lagging chromosomes compared with 7.95 ± 3.44% in control cells (Supplemental Figure 3, B and C). These findings suggest that Gravin loss contributes to increased chromosome segregation defects. We further tested whether lagging chromosomes can be rescued in cells when Gravin is reintroduced (Figure 5, A and B; Supplemental Figure S3D). We found that cells lacking Gravin or expressing Gravin T766A contained lagging chromosomes compared with rescue cells with wild-type Gravin, suggesting that the binding of Gravin to PLK1 is essential for proper chromosome alignment during metaphase.

Since chromosome misalignment can result in formation of micronuclei (Crasta *et al.*, 2012), we examined whether disrupting the

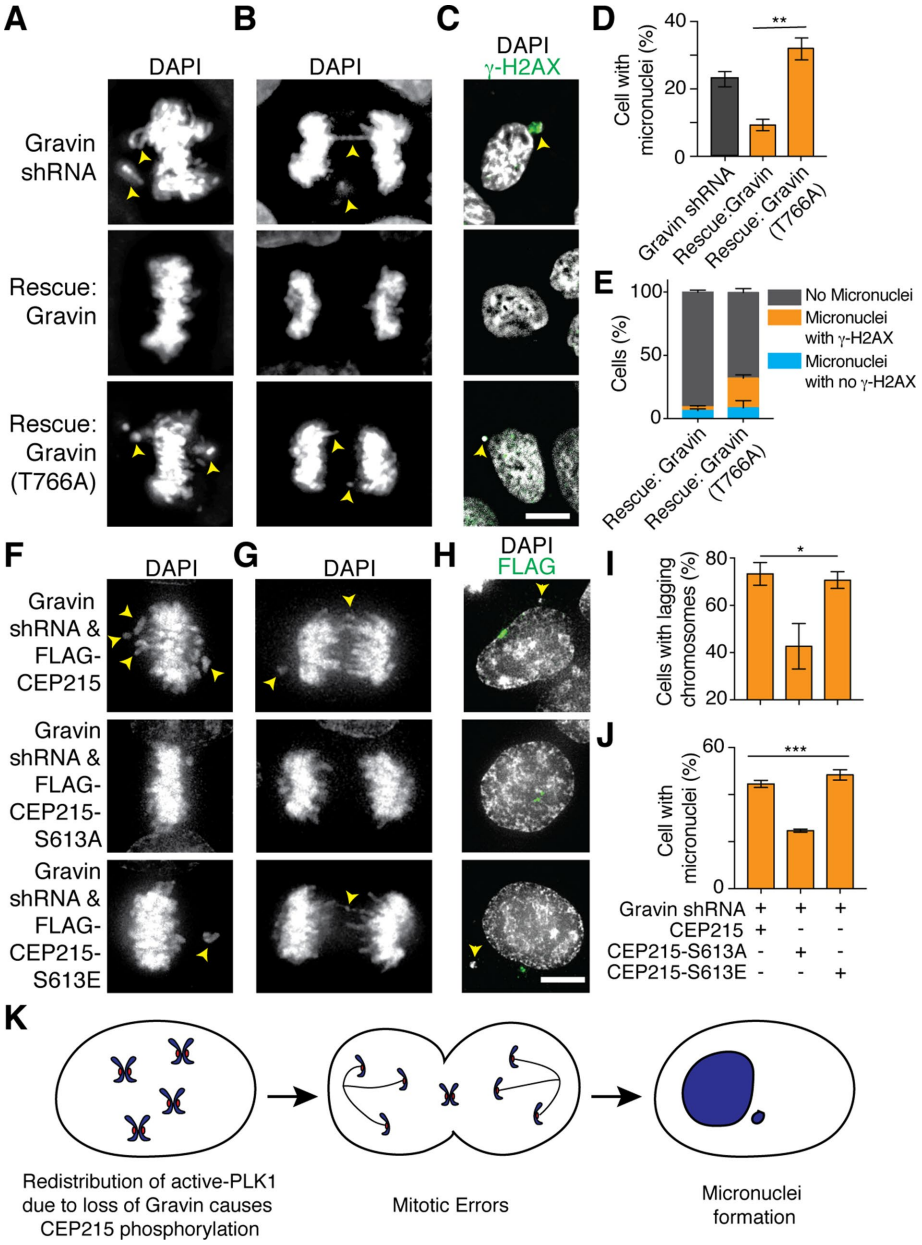

FIGURE 5: Gravin loss and increased phosphorylation of CEP215 results in higher incidence of cells containing micronuclei. (A–C) Wide-field deconvolved micrographs of Gravin shRNA, full-length Gravin rescue, and mutant T766A Gravin cells are presented as maximum projections. Cells were immunostained for DAPI (A, B, C white) and γ-H2AX (C, green). Bar, 5 μm. (D) Quantification of cells containing micronuclei (%) in Gravin shRNA–treated cells rescued with full-length Gravin or Gravin (T766A) over $n = 3$ experiments ± SEM; Student's t test p value = 0.0034. (E) Quantification of cells containing micronuclei with γ-H2AX (%) in Gravin shRNA cells rescued with full-length Gravin or Gravin (T766A) over $n = 3$ experiments ± SEM. (F–H) Deconvolved wide-field micrographs of Gravin shRNA–treated cells expressing FLAG-CEP215, FLAG-CEP215-S613A, or FLAG-CEP215-S613E presented as maximum projections. Cells were immunolabeled for DAPI (F, G, H, white) and FLAG (H, green). Bar, 5 μm. (I, J) Quantification of cells containing lagging chromosomes (I) and micronuclei (J) (%) in Gravin shRNA cells expressing FLAG-CEP215, FLAG-CEP215-S613A, or FLAG-CEP215-S613E. $n = 3$ experiments ± SEM, $n > 300$ cells, one-way ANOVA $p = 0.0290$ (I), $p = 0.0003$ (J). (K) Model summarizing that when Gravin is lost, a redistribution of active PLK1 leads to mitotic errors and subsequent formation of micronuclei.

Gravin–PLK1 interface resulted in increased formation of micronuclei. In Gravin-depleted cells we found that 22.87 ± 3.92% of cells formed micronuclei, whereas rescue with full-length wild-type Gravin led to a significant reduction in micronuclei formation (down to 9.3 ± 2.88%, Figure 5, C and D). When Gravin-depleted cells were rescued with Gravin-T766A, 32.03 ± 5.61% of cells displayed formation of micronuclei. To confirm that loss of Gravin resulted in increased formation of micronuclei, we compared wild-type and Gravin-null MEFs (Supplemental Figure S3, E and F). Gravin-null MEFs resulted in a twofold increase in formation of micronuclei compared with controls (Supplemental Figure S3F). These data suggest that disruption of the Gravin–PLK1 interface results in lagging chromosomes and micronuclei formation (modeled in Figure 5K). Previous studies suggested that micronuclei formed from lagging chromosomes develop DNA breaks (Leibowitz *et al.*, 2015). Since disrupting the Gravin–PLK1 binding interaction causes an increase in chromosome missegregation and formation of micronuclei (Figure 5, A–D), we examined whether these micronuclei had an increased incidence in developing DNA breaks by staining for γ-H2AX (Figure 5, C and E). Of cells rescued with Gravin-T766A that contained micronuclei, 76.37 ± 24.66% contained γ-H2AX-positive micronuclei compared with 33.33 ± 11.55% of wild-type Gravin rescue cells (Figure 5E).

CEP215 phosphorylation by PLK1 at serine-613 when Gravin is depleted (Figure 3, I–M) results in CEP215 disorganization at mitotic centrosomes (Figure 4, A–C). Thus, we tested in Gravin-depleted cells whether CEP215-S613A can alleviate chromosome missegregation errors and micronuclei formation compared with a phospho-mimetic mutant CEP215-S613E or wild-type CEP215 (Figure 5, F–J; Supplemental Figure S3G). The FLAG-tagged nonphosphorylatable mutant (S613A) and the FLAG-tagged phosphomimetic mutants (S613E) localize to mitotic spindle poles in control and Gravin-depleted cells (Supplemental Figure S3G) and to the interphase centrosome in Gravin-depleted cells (Figure 5H). We found that 73.33 ± 4.81% of cells expressing FLAG-CEP215 and 70.67 ± 3.53% of cells expressing FLAG-CEP215-S613E presented with lagging chromosomes, compared with 42.67 ± 9.62% in cells expressing FLAG-CEP215-S613A (Figure 5I). The cells expressing FLAG-CEP215 (47 ± 2.65%) or FLAG-CEP215-S613E (48.33 ± 2.19%) contained significantly more micronuclei than cells expressing FLAG-CEP215-S613A (24.67 ± 0.67%, Figure 5J). These data suggest that PLK1-dependent CEP215 phosphorylation at S613 leads to increased chromosome instability through the formation of lagging chromosomes and formation of micronuclei. Together, our findings suggest that blocking the ability

of Gravin to scaffold PLK1 causes an increase in DNA damage (Figure 5K). This is a potential mechanism by which chromosome instability can arise upon PLK1 deregulation in prostate cancer.

MATERIALS AND METHODS

Cell culture

3-D RWPE human prostate epithelial cells were grown in Keratinocyte SFM combo from Life Technologies/Fisher (cat. no. 17-005-042) with 60% Matrigel (Fisher cat. no. CB40234C; Corning no. 356237). 2-D PLK1-GFP RPE, GFP-H2B HeLa (Hehnly and Doxsey, 2014), mouse embryonic fibroblasts (MEFs) isolated from wild type and Gravin null mice, and human embryonic kidney (HEK) 293ad cells were grown in 1× DMEM (Life Technologies) supplemented with 10% Seradigm fetal bovine serum (FBS; VWR) and 1% penicillin–streptomycin (10,000 U/ml) (Life Technologies). Phoenix-AMPHO cells were used for viral production in Gravin rescue experiments, grown in 1X DMEM (Life Technologies) supplemented with 10% FBS (Sigma) and 1% penicillin–streptomycin (10,000 U/ml) (Life Technologies). All cultures were maintained at 37°C with 5% CO_2.

Human primary prostate cancer epithelial cells (PCa1, PCa3) were grown as 3-D-organoid cultures (Gao *et al*., 2014). Cells were plated in 200-µl DMEM/F12 containing supplements in a multiwell plate (Ibidi cell chambers #80827; PCa1 and PCa3 at 3000 cells/well) coated with collagen type II. Media supplements included epithelial growth factor (EGF), R-spondin 1, noggin, FGF10, FGF2, dihydrotestosterone (DHT), nicotinamide, the TGF-b/Alk inhibitor A83-01, the p38 MAK kinase inhibitor SB202190, the ROCK inhibitor Y-27632, B27 additive, *N*-acetyl-L-cysteine, glutamax, HEPES, and primocin. Following seeding, media were removed and cells overlaid with 200 µl of 50% GFR (growth factor–reduced) matrigel (GFR-matrigel from Fisher cat. no. CB40230C; Corning no. 356231) and 50% mixture.

shRNA and FRET constructs

Cells depleted of Gravin were made using a lentivirus-infected shRNA specific to Gravin (AKAP12 [Gravin] shRNA sc-40305-v). Control cells were treated with control shRNA (sc-108080). Gravin rescue experiments were performed using the wild-type and phospho-dead mutant T766A of the murine Gravin (SSECKS) gene. FRET experiments were performed using a PLK1 FRET biosensor containing a PLK1 specific c-jun substrate (Liu *et al*., 2012). To examine PLK1 activity specifically at mitotic centrosomes, a localized PLK1 FRET-biosensor was constructed by fusing the above FRET biosensor to the PACT domain (human pericentrin-kendrin) using a 10–amino acid linker (R-A-Q-A-S-N-S-G-R-P) as done for kinetochores in Liu *et al*. (2012). All constructs were verified through sequencing.

Antibodies and chemical inhibitors

For Western blot analysis and immunofluorescence imaging, the following antibodies were used: phospho-Histone H3 (Ser10, 1:200; Cell Signaling 9701S), mouse anti-PLK1 (E-2, 1:250; Santa Cruz sc-55504), rabbit anti-PLK1 (1:100; Cell Signaling #4513S), mouse anti-Centrin (1:1,000; EMD Millipore 04-1624), mouse anti-Gravin (1:250; Sigma Aldrich 45-G3795), anti–α-tubulin conjugated with FITC (1:250; Sigma Aldrich F2168), Actinred 555vReady Probes reagent (Thermo Fisher Scientific R37112), NucBlue fixed cell stain from Ready Probes (Thermo Fisher Scientific R37606), rabbit anti–γ-histone H2A.X (Ser 139, γ-H2AX, 1:500; Cell Signaling 9718S), anti-CEP215 (1:500; Bethyl Laboratories IHC-00063), anti–acetylated tubulin (1:500; Sigma 45-T6793), and phosphoserine/phosphothreonine (1:40; Fisher Scientific 01-672-764). Horseradish peroxidase (HRP)-conjugated antibodies included donkey anti-mouse immunoglobulin G (IgG) (H+L; Jackson ImmunoResearch Labs 715-035-150), donkey anti-rabbit IgG (H+L; Jackson ImmunoResearch Labs 711-035-152), and mouse anti-GAPDH (1:10,000; Sigma Aldrich 45-G9295). Fluorescent secondary antibodies included AlexaFluor donkey anti-mouse 488 (Life Technologies A21202), 568 (Life Technologies A10037), and 647 (Life Technologies A31571) and AlexaFluor donkey anti-rabbit 488 (Life Technologies A21206), 568 (Life Technologies A10042), and 647 (Life Technologies A31573).

Immunofluorescence for 3-D cultures/2-D cultures

Using a pipette, as in Hung *et al*. (2016), media were carefully removed from cultures. Cultures were rinsed with PBS and fixed with 4% paraformaldehyde (PFA) at room temperature for 30 min with light shaking. The PFA was carefully removed and replaced with fresh PFA for an additional 30 min with light shaking. After the PFA was removed, 50 mM NH_4Cl was added for 10 min. Cells were washed with PBS for 30 min with light shaking and then treated for 5 min with 0.1% Triton-X, blocked with PBSΔT (PBS, 1% BSA, 0.5% Triton X-100), and incubated with primary antibodies for 4 h at room temperature. Cultures were washed three times with PBSΔT and incubated with secondary antibodies for 4 h at room temperature. Cultures were kept in PBS containing DABCO (1,4-diazabicyclo[2.2.2] octane) antifade reagent (200 mM) for imaging.

Cells were plated on #1.5 coverslips until they reached 90% confluence and fixed using methanol (–20°C). Cells were rehydrated in PBS before blocking in PBSΔT for 30 min. Primary antibodies diluted in PBSΔT were added to coverslips and incubated for 1 h at room temperature, followed by 10 washes with PBSΔT, secondary antibodies for 1 h at room temperature, and then 10 washes with PBSΔT. Coverslips were rinsed with diH_2O and mounted on glass slides using Prolong Diamond with 4,6-diamidino-2-phenylindole (DAPI) mounting media.

Imaging

Cells were imaged using either a Leica DMi8 STP800 (Leica, Bannockburn, IL) equipped with a Lumencor SPECTRA X with a Hamamatsu ORCAflash 4.0 V2 CMOS C11440-22CU camera using either a 40 × 1.15 N.A. Lambda S LWD objective or 100 ×/1.4 N.A. HC Pl Apo oil emersion objective and Metamorph software to acquire images or a PerkinElmer Ultraview VoX spinning disc confocal system on a Nikon Eclipse Ti-E microscope using a Hammamatsu C9100-50 EMCCD camera and a 100 ×/1.4 N.A. Apo oil emersion objective using Volocity software. Superresolution 3D-SIM images were acquired on a DeltaVision OMX V4 (GE Healthcare) equipped with a 60 ×/1.42 N.A. PlanApo oil immersion lens (Olympus), 405-, 488-, 568-, and 642-nm solid-state lasers, and sCMOS cameras (pco.edge). Image stacks of 5–6 µm with 0.125-µm-thick *z*-sections and 15 images per optical slice (three angles and five phases) were acquired using immersion oil with a refractive index 1.518. Images were reconstructed using Wiener filter settings of 0.003 and optical transfer functions measured specifically for each channel with SoftWoRx 6.1.3 (GE Healthcare). Images from different color channels were registered using parameters generated from a gold grid registration slide (GE Healthcare) and SoftWoRx 6.1.3 (GE Healthcare). STED imaging was performed using a Leica TCS SP8 (Leica, Bannockburn, IL) equipped with STED 3X, a supercontinuum laser (white light laser 470–670 nm) for excitation, 592/546/600-nm STED depletion lasers, and an HCS PL APO 100x/1.40 oil STED white objective. Images were acquired using the Leica LAS software and postimage processing of STED images was performed using SVI Huygens deconvolution software.

FRAP experiments were performed using a Leica SP5 scanning confocal microscope (Leica, Bannockburn, IL) with an HCX Plan Apochromat 63 ×/1.40-0.06 N.A. OIL objective or the PerkinElmer Ultraview VoX spinning disc confocal system on a Nikon Eclipse Ti-E microscope. With the Leica SP5 the LAS AF (Leica application suite advanced fluorescence) software (Leica) FRAP wizard was used to acquire images. The ImageJ FRAP calculator macro plug-in was used to generate FRAP curves and generate half-life and immobile fraction values. Graphs were then produced in Prism GraphPad software.

Fluorescence resonance energy transfer

HEK293ad cells were transfected with a PLK1 FRET or a PLK1 FRET-PACT sensor using Mirus Bio TransIT-LT1 transfection reagent (Hukasova *et al.*, 2012; Liu *et al.*, 2012; Bruinsma *et al.*, 2015). After 24 h, cells were synched for 8 h using 100 nM nocodazole and released. To inhibit PLK1 cells were treated with 100 nM BI2536 for 20 min. Images were acquired on a Leica DMi8 STP800 (Leica, Bannockburn, IL) using a 63 ×/1.4 N.A. HC Pl Apo oil emersion objective. The $YFP^{ex} \rightarrow YFP^{em}$/$CFP^{ex} \rightarrow YFP^{em}$ emission ratio in each image was calculated after background subtraction and averaged over multiple cells. The FRET ratio was calculated using an ImageJ Ratio-Plus plugin. Experiments were repeated multiple times with similar results.

Mitotic centrosome isolation

HEK 293ad cells were treated with 100 nM nocodazole for 18 h. A mitotic shake-off was then performed, and centrosome isolation was carried out as described in Hung *et al.* (2015). In short, HEK293ad cells were treated with 20 µg/ml cytochalasin D and 10 µg/ml nocodazole for 2 h. Cells were then washed with the following buffers in order: 1X PBS, 0.1%PBS:8% wt/wt sucrose, 8% wt/wt sucrose, lysis buffer (LB) (1 mM Tris-HCl, 8 mM BME). Cells were then treated with 1 ml (per 100 mm plate) LB + 0.5% NP40 containing phosphatase inhibitors at 4°C for 2 min on rocker. Supernatants were collected and centrifuged at 1500 × *g* for 6 min at 4°C. The supernatants were then transferred to tubes containing 5 ml Ficoll (20% diluted in PE buffer [10 mM PIPES, 1 mM EDTA, 8 mM BME]) and centrifuged at 13,000 × *g* for 15 min at 4°C, and the Ficoll-PE interface (~150 µl) was collected. The interface was diluted in PE buffer containing phosphatase inhibitors and isolated onto coverslips by centrifugation. Mitotic centrosomes were fixed with ice-cold methanol and immunostained for pS/pT and centrin.

Immunoprecipitation

HEK293ad cells were transfected with 5 µg (per 100 mm plate) FLAG-CEP215. After 48 h, cells were lysed using ice-cold HEPES lysis buffer (25 mM HEPES, 150 mM NaCl, 0.5% Triton X-100, 1 mM EDTA, 1 mM ethylene glycol-bis(β-aminoethylether)-*N*,*N*,*N*′,*N*′-tetraacetic acid [EGTA], 2% glycerol, 10 mM NaF) and then incubated on ice for 10 min, and postnuclear supernatant was collected. A quantity of 600 µg–1 mg protein was incubated with anti-FLAG M2 affinity gel beads (Sigma) for 1.5 h at 4°C on rotator. Beads were washed twice with lysis buffer, and isolated beads were boiled in 30-µl sample buffer before Western blot analysis.

Ice treatment

HEK293ad cells treated with either control shRNA or Gravin shRNA were placed in Leibovitz's L-15 media (ThermoFisher #21083027) and placed on ice. After 5 min, the cells were washed in PBS and fixed in ice-cold methanol at –20°C for 10 min. Cells were then immunolabeled and imaged for analysis.

Microtubule renucleation assay

HEK293ad cells were treated with 10 µg nocodazole in media for 1 h. Cells were then washed three times with PBS before being placed in media at 37°C for times indicated. Cells were fixed using ice-cold methanol at –20°C, immunolabeled, and imaged for analysis.

Image analysis

A series of 0.2 µm Z-steps of cell volumes are presented as maximum projections using ImageJ. AutoQuant deconvolution was used on wide-field images using Metamorph software. Integrated intensities were measured on sum projections as described in Hoffman *et al.* (2001). To measure integrated intensity on either isolated centrosomes or mitotic centrosomes, circular regions of interest (ROIs) were drawn. The larger ROI (ROI^L) is used to measure background whereas the center smaller ROI (ROI^S) measures signal. The following equation was used: integrated intensity of ROI^L – ((integrated intensity of ROI^S – integrated intensity of ROI^L)×(area ROI^L/(area ROI^S– area ROI^L))) (Hehnly and Doxsey, 2014). Line scans were performed by calculating the normalized fluorescence intensity across a single line. Graphs and statistical analysis (unpaired Student's *t* tests or analysis of variance [ANOVA] as labeled) were completed using Graphpad Prism software. Error bars represent ± SEM; $p < 0.05$ was considered to be statistically significant. All images were set to a resolution of 300 DPI or greater after image analysis from raw data.

ACKNOWLEDGMENTS

The work was supported by National Institutes of Health Grant R00GM107355 (to H.H.), Department of Defense Grant PC160083 (to H.H.), the Carol Baldwin Foundation of Central New York (to H.H.), National Cancer Institute R01 CA161018 (to L.K.), and Department of Health Prostate Cancer Hypothesis Development RFA 1410200115 (to L.K. and H.H.). We thank René Medema for providing us with the PLK1-FRET biosensor plasmid, Patrina Pellett (previously at G.E., currently at Oxford Nanoimaging) for assistance obtaining SIM images, and Geoff Daniels and Jessica Shivas (Leica) for assistance obtaining STED images. We thank Wenyi Feng (Upstate Medical University) and Jeff Amack (Upstate Medical University) for critical feedback.

REFERENCES

Bruinsma W, Aprelia M, Kool J, Macurek L, Lindqvist A, Medema RH (2015). Spatial separation of Plk1 phosphorylation and activity. Front Oncol 5, 1–8.

Canton DA, Keene CD, Swinney K, Langeberg LK, Nguyen V, Pelletier L, Pawson T, Wordeman L, Stella N, Scott JD (2012). Gravin is a transitory effector of Polo-like kinase 1 during cell division. Mol Cell 48, 547–559.

Chan EHY, Santamaria A, Silljé HHW, Nigg EA (2008). Plk1 regulates mitotic Aurora A function through betaTrCP-dependent degradation of hBora. Chromosoma 117, 457–469.

Crasta K, Ganem NJ, Dagher R, Lantermann AB, Ivanova EV, Pan Y, Nezi L, Protopopov A, Chowdhury D, Pellman D (2012). DNA breaks and chromosome pulverization from errors in mitosis. Nature 482, 53–58.

Deeraksa A, Pan J, Sha Y, Liu X-D, Eissa N, Lin S-H, Yu-Lee L-Y (2013). Plk1 is upregulated in androgen-insensitive prostate cancer cells and its inhibition leads to necroptosis. Oncogene 32, 2973–2983.

Fong K-W, Choi Y-K, Rattner JB, Qi RZ (2008). CDK5RAP2 is a pericentriolar protein that functions in centrosomal attachment of the γ-tubulin ring complex. Mol Biol Cell 19, 115–125.

Gao D *et al.* (2014). Organoid cultures derived from patients with advanced prostate cancer. Cell 159, 176–187.

Gelman IH (2010). Emerging roles for SSeCKS/Gravin/AKAP12 in the control of cell proliferation, cancer malignancy, and barriergenesis. Genes Cancer 1, 1147–1156.

Hehnly H, Canton D, Bucko P, Langeberg LK, Ogier L, Gelman I, Santana LF, Wordeman L, Scott JD (2015). A mitotic kinase scaffold depleted in testicular seminomas impacts spindle orientation in germ line stem cells. Elife 4, e09384.
Hehnly H, Doxsey S (2014). Rab11 endosomes contribute to mitotic spindle organization and orientation. Dev Cell 28, 497–507.
Hoffman DB, Pearson CG, Yen TJ, Howell BJ, Salmon ED (2001). Microtubule-dependent changes in assembly of microtubule motor proteins and mitotic spindle checkpoint proteins at PtK1 kinetochores. Mol Biol Cell 12, 1995–2009.
Holland AJ, Cleveland DW (2012). Chromoanagenesis and cancer: mechanisms and consequences of localized, complex chromosomal rearrangements. Nat Med 18, 1630–1638.
Hukasova E, Silva Cascales H, Kumar SR, Lindqvist A (2012). Monitoring kinase and phosphatase activities through the cell cycle by ratiometric FRET. J Vis Exp e3410.
Hung H-F, Hehnly H, Doxsey S (2015). Methods to analyze novel liaisons between endosomes and centrosomes. Biophys Methods Cell Biol 130, 47–58.
Hung HF, Hehnly H, Doxsey S (2016). The mother centriole appendage protein cenexin modulates lumen formation through spindle orientation. Curr Biol 26, 793–801.
Joukov V, Walter JC, De Nicolo A (2014). The Cep192-organized Aurora A-Plk1 cascade is essential for centrosome cycle and bipolar spindle assembly. Mol Cell 55, 578–591.
Kishi K, van Vugt MATM, Okamoto K, Hayashi Y, Yaffe MB (2009). Functional dynamics of Polo-like kinase 1 at the centrosome. Mol Cell Biol 29, 3134–3150.
Leibowitz ML, Zhang C-Z, Pellman D (2015). Chromothripsis: a new mechanism for rapid karyotype evolution. Annu Rev Genet 49, 183–211.
Lera RF, Burkard ME (2012). High mitotic activity of Polo-like kinase 1 is required for chromosome segregation and genomic integrity in human epithelial cells. J Biol Chem 287, 42812–42825.
Liu D, Davydenko O, Lampson MA (2012). Polo-like kinase-1 regulates kinetochore-microtubule dynamics and spindle checkpoint silencing. J Cell Biol 198, 491–499.
Lowery DM, Clauser KR, Hjerrild M, Lim D, Alexander J, Kishi K, Ong S-E, Gammeltoft S, Carr SA, Yaffe MB (2007). Proteomic screen defines the Polo-box domain interactome and identifies Rock2 as a Plk1 substrate. EMBO J 26, 2262–2273.
Macůrek L, Lindqvist A, Lim D, Lampson MA, Klompmaker R, Freire R, Clouin C, Taylor SS, Yaffe MB, Medema RH (2008). Polo-like kinase-1 is activated by aurora A to promote checkpoint recovery. Nature 455, 119–123.
Pan S-H, Tai C-C, Lin C-S, Hsu W-B, Chou S-F, Lai C-C, Chen J-Y, Tien H-F, Lee F-Y, Wang W-B (2009). Epstein–Barr virus nuclear antigen 2 disrupts mitotic checkpoint and causes chromosomal instability. Carcinogenesis 30, 366–375.
Paschal CR, Maciejowski J, Jallepalli P V (2012). A stringent requirement for Plk1 T210 phosphorylation during K-fiber assembly and chromosome congression. Chromosoma 121, 565–572.
Santamaria A, Wang B, Elowe S, Malik R, Zhang F, Bauer M, Schmidt A, Silljé HHW, Körner R, Nigg EA (2011). The Plk1-dependent phosphoproteome of the early mitotic spindle. Mol Cell Proteomics 10, M110.004457.
Sir JH, Pütz M, Daly O, Morrison CG, Dunning M, Kilmartin JV, Gergely F (2013). Loss of centrioles causes chromosomal instability in vertebrate somatic cells. J Cell Biol 203, 747–756.
Zitouni S, Nabais C, Jana SC, Guerrero A, Bettencourt-Dias M (2014). Polo-like kinases: structural variations lead to multiple functions. Nat Rev Mol Cell Biol 15, 433–452.